JCI The Journal of Clinical Investigation

Lipocalin 2 is essential for chronic kidney disease progression in mice and humans

Amandine Viau, … , Jonathan Barasch, Fabiola Terzi

J Clin Invest. 2010;120(11):4065-4076. https://doi.org/10.1172/JCI42004.

Research Article **Nephrology**

Mechanisms of progression of chronic kidney disease (CKD), a major health care burden, are poorly understood. EGFR stimulates CKD progression, but the molecular networks that mediate its biological effects remain unknown. We recently showed that the severity of renal lesions after nephron reduction varied substantially among mouse strains and required activation of EGFR. Here, we utilized two mouse strains that react differently to nephron reduction — FVB/N mice, which develop severe renal lesions, and B6D2F1 mice, which are resistant to early deterioration — coupled with genome-wide expression to elucidate the molecular nature of CKD progression. Our results showed that lipocalin 2 (*Lcn2*, also known as neutrophil gelatinase–associated lipocalin [NGAL]), the most highly upregulated gene in the FVB/N strain, was not simply a marker of renal lesions, but an active player in disease progression. In fact, the severity of renal lesions was dramatically reduced in $Lcn2^{-/-}$ mice. We discovered that Lcn2 expression increased upon EGFR activation and that Lcn2 mediated its mitogenic effect during renal deterioration. EGFR inhibition prevented Lcn2 upregulation and lesion development in mice expressing a dominant negative EGFR isoform, and hypoxia-inducible factor 1α (Hif-1α) was crucially required for EGFR-induced Lcn2 overexpression. Consistent with this, cell proliferation was dramatically reduced in $Lcn2^{-/-}$ mice. These data are relevant to human CKD, as we found that LCN2 was increased particularly in […]

Lipocalin 2 is essential for chronic kidney disease progression in mice and humans

Amandine Viau,[1] Khalil El Karoui,[1] Denise Laouari,[1] Martine Burtin,[1] Clément Nguyen,[1] Kiyoshi Mori,[2] Evangéline Pillebout,[1] Thorsten Berger,[3] Tak Wah Mak,[3] Bertrand Knebelmann,[1] Gérard Friedlander,[1] Jonathan Barasch,[2] and Fabiola Terzi[1]

[1]INSERM U845, Centre de Recherche "Croissance et Signalisation," Université Paris Descartes, Hôpital Necker Enfants Malades, Paris, France. [2]Department of Medicine, Columbia University, New York, New York, USA. [3]The Campbell Family Institute for Cancer Research, University Health Network, Toronto, Ontario, Canada.

Mechanisms of progression of chronic kidney disease (CKD), a major health care burden, are poorly understood. EGFR stimulates CKD progression, but the molecular networks that mediate its biological effects remain unknown. We recently showed that the severity of renal lesions after nephron reduction varied substantially among mouse strains and required activation of EGFR. Here, we utilized two mouse strains that react differently to nephron reduction — FVB/N mice, which develop severe renal lesions, and B6D2F1 mice, which are resistant to early deterioration — coupled with genome-wide expression to elucidate the molecular nature of CKD progression. Our results showed that lipocalin 2 (*Lcn2*, also known as neutrophil gelatinase–associated lipocalin [NGAL]), the most highly upregulated gene in the FVB/N strain, was not simply a marker of renal lesions, but an active player in disease progression. In fact, the severity of renal lesions was dramatically reduced in *Lcn2*$^{-/-}$ mice. We discovered that Lcn2 expression increased upon EGFR activation and that Lcn2 mediated its mitogenic effect during renal deterioration. EGFR inhibition prevented Lcn2 upregulation and lesion development in mice expressing a dominant negative EGFR isoform, and hypoxia-inducible factor 1α (Hif-1α) was crucially required for EGFR-induced Lcn2 overexpression. Consistent with this, cell proliferation was dramatically reduced in *Lcn2*$^{-/-}$ mice. These data are relevant to human CKD, as we found that LCN2 was increased particularly in patients who rapidly progressed to end-stage renal failure. Together our results uncover what we believe to be a novel function for Lcn2 and a critical pathway leading to progressive renal failure and cystogenesis.

Introduction

Regardless of the initial insult, human chronic kidney disease (CKD) is characterized by progressive destruction of the renal parenchyma and the loss of functional nephrons, which ultimately lead to end-stage renal failure (ESRF). CKD represents a worldwide concern: in the United States, 102,567 patients began dialysis in 2003 (341 patients/million per year) (1), and similar rates were found in developing countries and in particular ethnic groups (2). However, these numbers are a small fraction of the millions of patients who are thought to have some degree of renal impairment. In the United States, the prevalence of chronically reduced kidney function is 11% of adults (3). Understanding the pathophysiology of CKD progression is, therefore, a key challenge for medical planning.

The mechanisms of CKD progression are poorly understood. It has been shown that reduction of the number of functional nephrons triggers molecular and cellular events promoting compensatory growth of the remaining ones (4). In some cases, this compensatory process becomes pathological, with the development of renal lesions and ESRF. Although the pathophysiology of compensation and progression is complex, unregulated proliferation of glomerular, tubular, and interstitial cells may promote the development of glomerulosclerosis, tubular cysts, and interstitial fibrosis (5–7). The molecular programs that control this cascade of events are largely unknown.

Attempts to dissect the molecular basis of CKD have been facilitated by the development of several experimental models of renal deterioration. Among these, the remnant kidney model is a mainstay, since nephron reduction characterizes the evolution of most human CKD. Consequently, this model recapitulates many features of human CKD, including hypertension, proteinuria, and glomerular and tubulointerstitial lesions. Over the last 50 years, this model has led to the discovery of critical pathways and, more importantly, to the design of therapeutic strategies to slow the progression of CKD, such as the widely clinically used renin-angiotensin inhibitors (8).

More recently, studies in various mouse strains have highlighted the importance of genetic factors in the evolution of experimental nephron reduction (9–11). We previously showed that the course and extent of renal lesions following nephron reduction vary significantly between two mouse strains: whereas FVB/N mice develop severe lesions, (C57BL/6 × DBA2)F1 (hereafter referred to as B6D2F1) mice undergo compensation alone (12). Moreover, we observed that the development of renal lesions paralleled the extent of cell proliferation (12). In fact, once the compensatory growth is achieved, a second wave of cell proliferation occurs only in the FVB/N strain. Hence, this model offers a powerful tool to unravel the transcriptional programs and the critical mediators that are selectively activated long after nephron reduction to drive deterioration of the remaining nephrons.

In the present study, we performed an unbiased profiling of gene expression in the kidneys of the FVB/N and B6D2F1 mouse strains, 2 months after nephron reduction, when renal lesions develop and the second wave of cell proliferation is ongoing. We identified a critical mediator of progressive renal failure, namely the carrier protein lipocalin 2 (Lcn2, or neutrophil gelatinase-associated lipocalin [NGAL], siderocalin, 24p3, uterocalin), and uncovered what we believe to be a novel function of Lcn2. Moreover, we elucidated a unique molecular

Conflict of interest: The authors have declared that no conflict of interest exists.
Citation for this article: *J Clin Invest.* 2010;120(11):4065–4076. doi:10.1172/JCI42004.

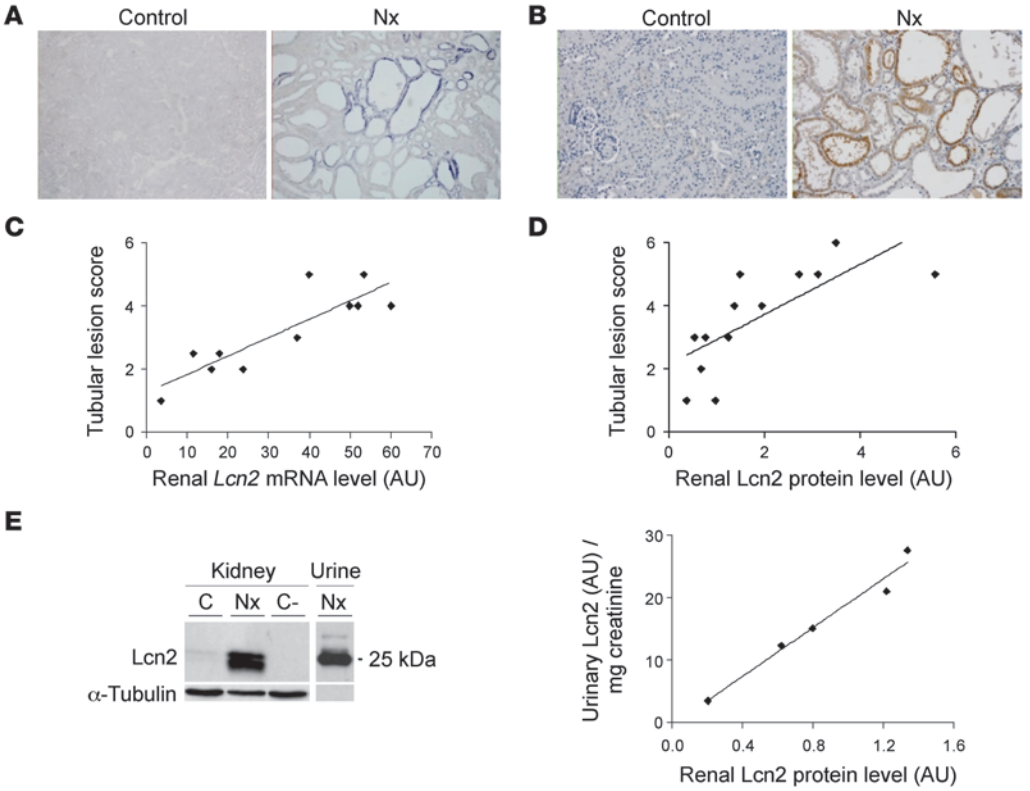

Figure 1

Lcn2 is overexpressed after nephron reduction in mice and correlates with lesion progression. (**A** and **B**) Lcn2 expression evaluated by (**A**) in situ hybridization (original magnification, ×100) and (**B**) immunohistochemistry (×200) in kidneys from sham-operated (control) and 75% Nx FVB/N mice 2 months after surgery. Representative images for each group ($n \geq 6$) are shown. (**C**) Correlation between renal *Lcn2* mRNA expression evaluated by real-time RT-PCR and tubular lesion score in FVB/N mice, 2 months after Nx ($r = 0.87$, $P < 0.001$). (**D**) Correlation between renal Lcn2 protein expression evaluated by Western blot and tubular lesion score in FVB/N mice, 2 months after Nx ($r = 0.74$, $P < 0.01$). (**E**) Urinary Lcn2 excretion significantly correlates with renal Lcn2 protein expression. Left panel: Western blot of renal and urinary Lcn2 protein in control (C) and Nx FVB/N mice. Protein extracts from kidney of Nx *Lcn2*$^{-/-}$ mice was used as negative control (C–). Right panel: Correlation between renal Lcn2 production and urinary Lcn2 excretion evaluated by Western blot ($r = 0.99$, $P < 0.01$).

pathway by which activation of EGFR results in Lcn2 expression, which then stimulates tubular proliferation and cystogenesis.

Results

Gene profiling. To elucidate the molecular pathways of CKD progression, we performed unbiased profiling of gene expression in remnant kidneys of two mouse strains that react differently to nephron reduction. Using microarrays containing 5,579 cDNAs, we found 70 genes whose expression levels differed significantly 2 months after nephron reduction ($P < 0.05$). Among these transcripts, 44 were upregulated (Supplemental Table 1; supplemental material available online with this article; doi:10.1172/JCI42004DS1) and 26 were downregulated (Supplemental Table 2) in damaged FVB/N kidneys as compared with well-preserved kidneys from B6D2F1 mice. Grouping these results by gene ontology category, we observed a range of functions for the 70 transcripts, although many of the downregulated mRNAs (38%) regulated metabolic processes (Supplemental Figure 1). The gene undergoing maximal transcriptional induction (9.95-fold change, $P = 0.008$) in the FVB/N lesion-prone strain was *Lcn2*.

Lcn2 correlates with lesion progression in mouse and human with CKD. Lcn2 is a member of the lipocalin superfamily (13), a family of proteins that transport hydrophobic molecules such as retinoids, fatty acids, and organic chelators of iron (14). Real-time RT-PCR confirmed that *Lcn2* mRNA increased 10-fold 2 months after nephron reduction in FVB/N but not in B6D2F1 mice, while it was almost undetectable in control animals (Supplemental Figure 2). In situ hybridization and immunohistochemistry corroborated these observations and showed a marked increase in *Lcn2* mRNA and protein in damaged kidneys of FVB/N mice (Figure 1, A and B). Lcn2 was predominantly found in proximal tubules and in a few ascending limbs of Henle's loops and collecting ducts (Supplemental Figure 3A). High magnification revealed that Lcn2 was mainly located in cytoplasmic granules at the subapical zone (Supplemental Figure 3B). By combining in situ hybridization and immunohistochemistry on serial sections, we found that a proportion of Lcn2 must have derived from the glomerular filtrate, since in some proximal tubules *Lcn2* mRNA staining was negative while anti-Lcn2 staining was markedly positive (in situ$^-$ and antibody$^+$). On the other hand, the majority of proximal epithelia that had undergone dilation and cystic transformation displayed both Lcn2 message and antibody staining (in situ$^+$ and antibody$^+$), indicating not only endocytosis of filtered protein but ongoing local synthesis and secretion of Lcn2 (Supplemental Figure 3C). Renal *Lcn2* mRNA (Figure 1C) and protein (Figure 1D) levels correlated with the intensity of tubular damage ($r = 0.87$, $P < 0.001$ and $r = 0.74$, $P < 0.01$ for mRNA and protein, respectively). In addition, we observed that renal Lcn2 protein content significant-

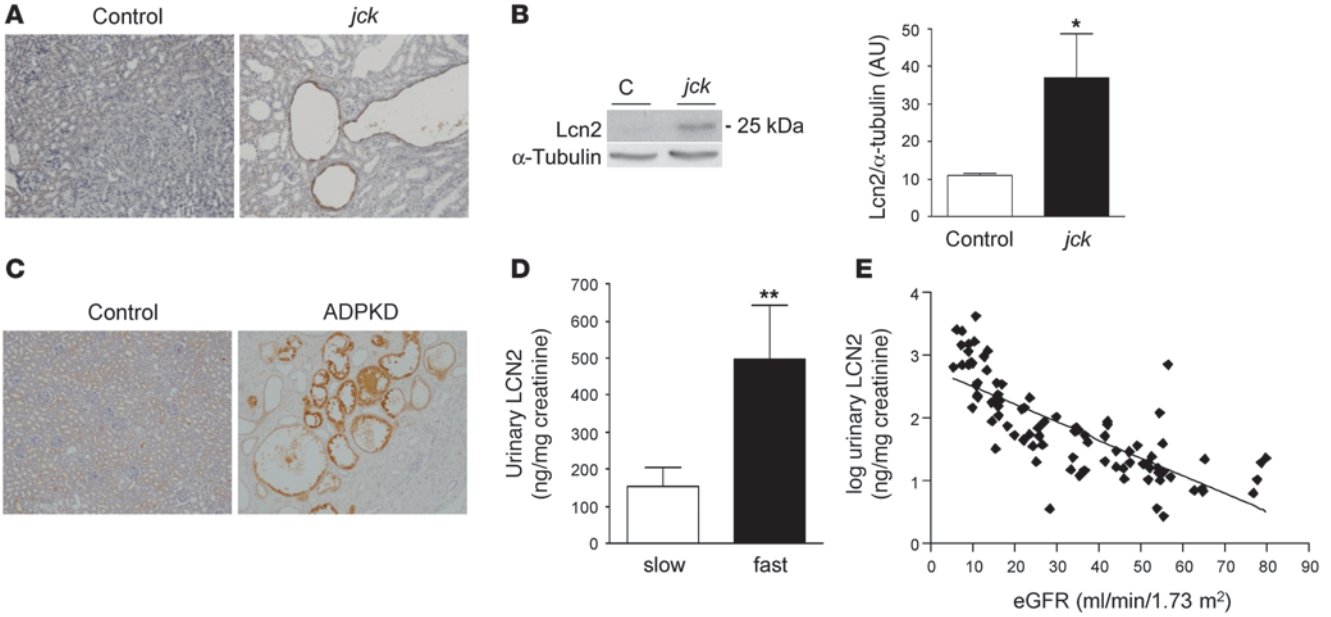

Figure 2

Lcn2 is overexpressed in polycystic kidney disease in mice and humans and correlates with CKD progression. (**A** and **B**) Lcn2 expression evaluated by (**A**) immunohistochemistry and (**B**) Western blot in kidneys from wild-type (control) and *jck* mice, 3 weeks after birth. Representative images and blots for each group ($n \geq 4$) are shown. Original magnification, ×200. (**C**) LCN2 staining in kidneys from controls ($n = 9$) and patients with ADPKD ($n = 9$). Original magnification, ×100. (**D**) Urinary LCN2 excretion in patients with slow progression (eGFR decline <4.5 ml/min/1.73 m^2 per year) as compared with fast progressors (eGFR decline >4.5 ml/min/1.73 m^2 per year) toward ESRF. (**E**) Urinary LCN2 excretion inversely correlates with eGFR in patients with ADPKD ($r = -0.77$, $P < 0.0001$). Data are mean ± SEM; $n = 4$–6 for mice and $n = 87$ for ADPKD patients. Mann-Whitney *U* test: **P* < 0.05, control versus *jck* mice; ***P* < 0.01 slow versus fast progressors.

ly correlated with Lcn2 excretion ($r = 0.99$, $P < 0.01$) (Figure 1E), suggesting that the kidney is the major source of urinary Lcn2.

A time course analysis of Lcn2 expression and renal morphology revealed that the increase in both *Lcn2* mRNA and protein levels preceded the development of renal lesions 4 weeks after nephron reduction (Supplemental Figure 4). Moreover, we confirmed that Lcn2 upregulation was associated with the progressive development of tubular dilations in another experimental model of CKD, the juvenile cystic kidney (*jck*) mice (Figure 2, A and B). Of note, these mice develop a form of polycystic kidney disease similar to human autosomal dominant polycystic kidney disease (ADPKD) (15). Last, in patients with ADPKD, who are similar to our model in displaying severe and progressive tubular dilations, LCN2 immunoreactivity was markedly increased, particularly in cysts (Figure 2C). Urinary LCN2 was most prominent in fast progressors toward ESRF rather than in slow progressors (see Methods) (496 ± 146 vs. 152 ± 52 ng/mg creatinine, $P < 0.01$) (Figure 2D), and it inversely correlated with residual estimated glomerular filtration rate (eGFR) ($r = -0.77$, $P < 0.0001$) (Figure 2E) and microalbuminuria ($r = 0.72$, $P < 0.0001$). Interestingly, LCN2 expression was also increased in renal tubules of kidneys from patients with either congenital nephron deficit, a pathological condition very similar to nephron reduction, or IgA nephropathy, the most common primary form of CKD (Supplemental Figure 5). Our findings in mice and humans together with recent works (16–18) suggested that Lcn2 might participate in the pathogenesis of cysts and CKD.

Lcn2 gene inactivation prevents lesion development and cyst formation. To determine the role of Lcn2 in progressive CKD, we performed 75% nephron reduction (Nx) in *Lcn2*$^{-/-}$ mice (19). To this end, we first introduced the *Lcn2* mutated allele in the lesion-prone (FVB/N) background. The *Lcn2*$^{-/-}$ FVB/N mice reproduced normally and had no apparent phenotype under physiological conditions (data not shown). As expected, 2 months after nephron reduction, wild-type mice developed severe renal lesions, mainly consisting of glomerulosclerosis, tubular atrophy, and cystic dilation, mild interstitial fibrosis, and multifocal mononuclear cell infiltration (Figure 3A). However, the frequency and severity of renal lesions were dramatically reduced in *Lcn2*$^{-/-}$ mice. Quantification showed that *Lcn2*$^{-/-}$ mice had considerably fewer glomerular, tubular, and interstitial lesions as compared with wild-type littermates (Figure 3A). Notably, there were fewer tubular dilations and no cysts in *Lcn2*$^{-/-}$ mice. Consistent with these findings, renal function was better preserved in *Lcn2*$^{-/-}$ mice as compared with wild-type littermates, 2 months after nephron reduction. Serum creatinine and blood urea nitrogen were 5 ± 0.5, 18 ± 2.6, and 11 ± 0.6 μmol/l ($P < 0.01$) and 29 ± 1, 109 ± 15, and 65 ± 4 mg/dl ($P < 0.01$) in control, Nx *Lcn2*$^{+/+}$, and Nx *Lcn2*$^{-/-}$ mice, respectively (Supplemental Figure 6, A and B). As expected, mean arterial blood pressure significantly increased in wild-type mice as compared with control animals (135 ± 7.5 and 116 ± 3.4 mmHg, $P < 0.05$) 2 months after nephron reduction. The increase was of the same magnitude in *Lcn2*$^{-/-}$ mice (143 ± 2.2 mmHg). Development of renal lesions was accompanied by severe proteinuria in wild-type mice (6.16 ± 1.21 vs. 0.003 ± 0.001 mg/d in Nx and control mice, respectively, $P < 0.001$), whereas proteinuria was substantially decreased in *Lcn2*$^{-/-}$ animals (3.30 ± 1.03 mg/d, $P < 0.05$) (Supplemental Figure 6C). Of note, *Lcn2* inactivation did not change the course of nephron reduction in lesion-resistant C57BL/6 mice (Figure 4).

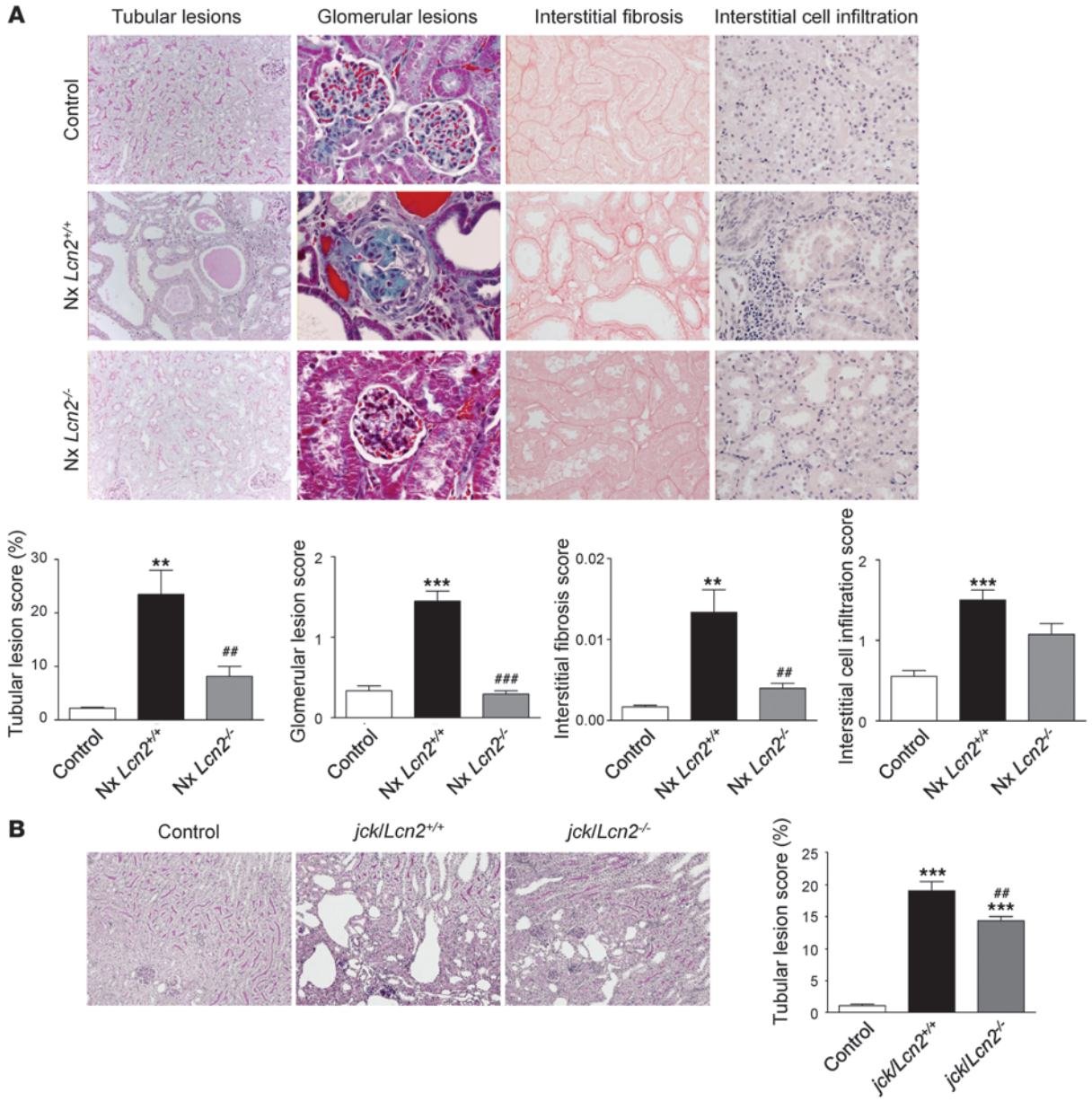

Figure 3

Lcn2 deficiency protects from the development of renal lesions. (**A**) Morphology and lesion scores of kidneys from control, 75% Nx *Lcn2*$^{+/+}$, and *Lcn2*$^{-/-}$ FVB/N mice, 2 months after nephron reduction. Original magnification, ×200, ×600, and ×400 for tubular, glomerular, and interstitial lesions, respectively. (**B**) Morphology and cystic surface of kidneys from control, *jck*/*Lcn2*$^{+/+}$, and *jck*/*Lcn2*$^{-/-}$ mice, 3 weeks after birth. Original magnification, ×200. Because no differences were detected between wild-type and mutant control mice, results for only 1 group are shown. Data are mean ± SEM; n = 4–6, 10–12, and 5–6 for control, Nx, and *jck* mice, respectively. ANOVA followed by Tukey-Kramer test: $^{**}P < 0.01$, $^{***}P < 0.001$, control versus Nx or *jck* mice; $^{\#\#}P < 0.01$, $^{\#\#\#}P < 0.001$, *Lcn2*$^{+/+}$ versus *Lcn2*$^{-/-}$.

To confirm the beneficial effect of *Lcn2* gene inactivation in renal deterioration and cyst formation, we bred *Lcn2*$^{-/-}$ mice with the *jck* mice. Notably, the severity of renal lesions was substantially reduced in double mutant *jck*/*Lcn2*$^{-/-}$ mice (Figure 3B). Quantification showed that the tubular dilation score was significantly lower in double mutant mice as compared with *jck* littermates 3 weeks after birth (Figure 3B). Collectively, these results demonstrated that Lcn2 is an effector of renal damage during CKD progression.

Iron accumulation does not account for progressive renal dysfunction. We next aimed at elucidating the mechanisms underlying the lesion-promoting effect of Lcn2. Lcn2 might act through iron mobilization (20). In fact, abnormal levels of iron accumulate in kidneys during CKD, where it may participate in the deterioration process (21, 22). Perls staining confirmed that iron content increased in damaged tubules 2 months after nephron reduction. However, iron accumulation was similar in remnant kidneys of *Lcn2*$^{-/-}$ mice as compared with wild-type littermates (Supplemental Figure 7). More importantly,

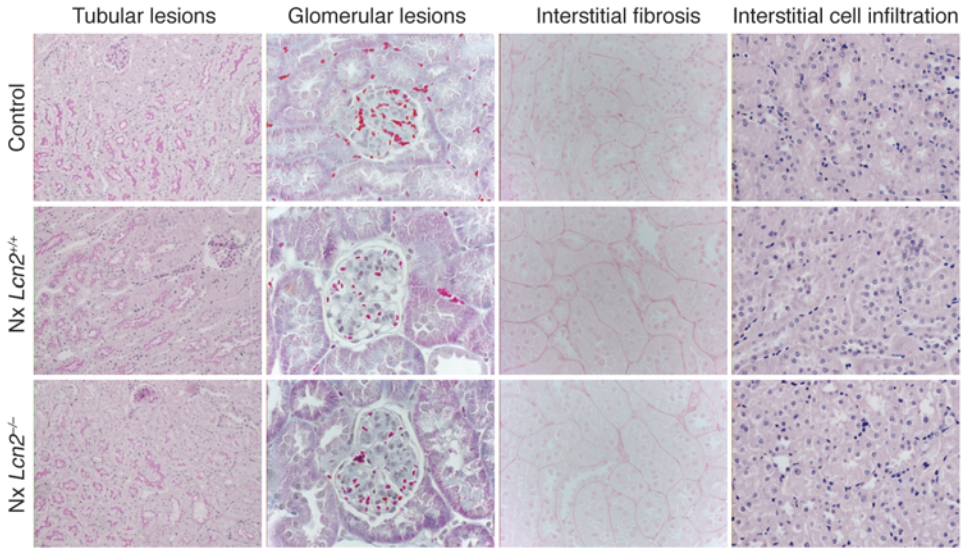

Figure 4
Lcn2 inactivation does not affect the response to nephron reduction in the lesion-resistant C57BL/6 mice. Morphology of kidneys from control, 75% Nx *Lcn2*$^{+/+}$, and *Lcn2*$^{-/-}$ C57BL/6 mice, 2 months after surgery. Original magnification, ×200, ×600, and ×400 for tubular, glomerular, and interstitial lesions, respectively. Because no differences were detected between wild-type and mutant control mice, results for only 1 group are shown. n = 4–6 and 8–10 for control and Nx mice, respectively.

chelation of iron by desferrioxamine (DFO) (Figure 5A) unexpectedly worsened renal disease in FVB/N mice (Figure 5B). In particular, tubular dilations were more severe and diffuse in mice treated with DFO 2 months after nephron reduction. Notably, *Lcn2* mRNA and protein expression were dramatically increased in kidneys of DFO-treated animals as compared with vehicle-treated counterparts (Figure 5, C and D). Proliferation of tubular cells was also significantly enhanced 2 months after nephron reduction in DFO-treated mice (Figure 5E). Hence, whereas iron deposited in the proximal tubules does not account for renal deterioration in our model, the experiments with DFO clearly show that manipulating Lcn2 levels is tightly correlated with hyperproliferation and progressive damage.

Lcn2 is a target of EGFR signaling. It is known that cell proliferation contributes to the development of renal lesions, and particularly to cystogenesis (23). Previous studies have suggested that Lcn2 can be induced by a number of growth factors that stimulate tubular cell proliferation (24). Among these, EGFR is of particular interest, since it is critical in the evolution of CKD (25). We therefore hypothesized that Lcn2 could act downstream of EGFR and mediate its growth effects. To investigate this hypothesis, we first treated renal tubular mIMCD-3 cells with EGF. Western blot analysis revealed that Lcn2 protein levels were markedly increased after addition of EGF (Figure 6A). Quantitative RT-PCR showed that *Lcn2* mRNA levels paralleled the increase of the protein in EGF-treated cells (Figure 6B), indicating that the *Lcn2* gene is transcriptionally regulated by EGFR. To validate these findings in vivo, we took advantage of a line of transgenic mice that overexpresses a dominant negative EGFR isoform (EGFR-M) selectively in proximal tubular cells (26). Inhibition of EGFR prevented the increase in *Lcn2* mRNA in remnant kidneys of transgenic mice, 2 months after nephron reduction (Figure 6C). Consistently, the severity of renal lesions was substantially reduced in EGFR-M mice as compared with wild-type littermates (Figure 6D).

Hif-1α is a critical intermediate between EGFR and Lcn2. We next tried to identify the factors that account for *Lcn2* transcription upon EGFR activation. The observation that DFO dramatically stimulated Lcn2 expression after nephron reduction suggested that hypoxia-inducible factors (HIFs) might play a role. In fact, by inhibiting Fe^{2+}-dependent prolyl hydroxylases, DFO stabilizes Hif-1α and Hif-2α (27). Interestingly, our results showed that Hif-1α protein levels increased in damaged kidneys of FVB/N mice 2 months after nephron reduction (Figure 7A). Since previous studies have shown that hypoxia may develop in damaged kidneys in CKD (28), we analyzed renal oxygenation 2 months after nephron reduction. Pimonidazole hypoxia probe failed to detect any positive tubules in remnant kidneys of FVB/N mice, with the exception of those located in the surgical scars (Figure 7B), demonstrating that hypoxia did not account for Hif-1α overexpression in our experimental model of CKD. In vitro experiments confirmed that EGF stimulated Hif-1α expression in renal mIMCD-3 cells. In fact, Hif-1α protein levels markedly increased upon EGF stimulation (Figure 7C). *Hif1a* mRNA levels, determined by real-time RT-PCR, changed neither in vivo after nephron reduction nor in vitro upon EGF treatment (data not shown), suggesting that Hif-1α is induced via a post-transcriptional mechanism. In addition, we observed that the increase in Hif-1α was specific, since the expression of Hif-2α changed neither in remnant kidneys nor in EGF-stimulated cells (Supplemental Figure 8). More importantly, we showed that Hif-1α silencing by siRNA partially inhibited Lcn2 expression both under basal conditions and, mainly, upon EGF stimulation in mIMCD-3 cell lines (Figure 7D), indicating that Hif-1α is a critical intermediate in EGFR-induced Lcn2 overexpression.

Lcn2 mediates the proliferative effect of EGFR. To next investigate whether Lcn2 mediated the mitogenic effect of EGFR, we established mIMCD-3 cell lines expressing Lcn2 shRNAs. Quantitative RT-PCR and Western blots revealed that *Lcn2* mRNA was depleted by 96% (Figure 8A), whereas the protein was undetectable (Figure 8B) in Lcn2-silenced cells. Interestingly, Lcn2 silencing completely abolished cell proliferation after the addition of EGF at different experimental time points (Figure 8C). Similar results were obtained by using different clones and a second shRNA targeting Lcn2 (data not shown). We found consistent results in our mouse model in vivo. In fact, *Lcn2* gene deletion prevented the increase in tubular cell proliferation 2 months after nephron reduction, as reflected in a significantly lower level of proliferating cell nuclear antigen–positive (PCNA-positive) tubular cells in remnant kidneys of *Lcn2*$^{-/-}$ mice as compared with wild-type littermates (Figure 8D). Notably, *Lcn2* gene inactivation did not inhibit the increase in cell proliferation in glomeruli (Figure 8E). These results were confirmed using an antibody directed against Ki-67, a protein selectively expressed in proliferat-

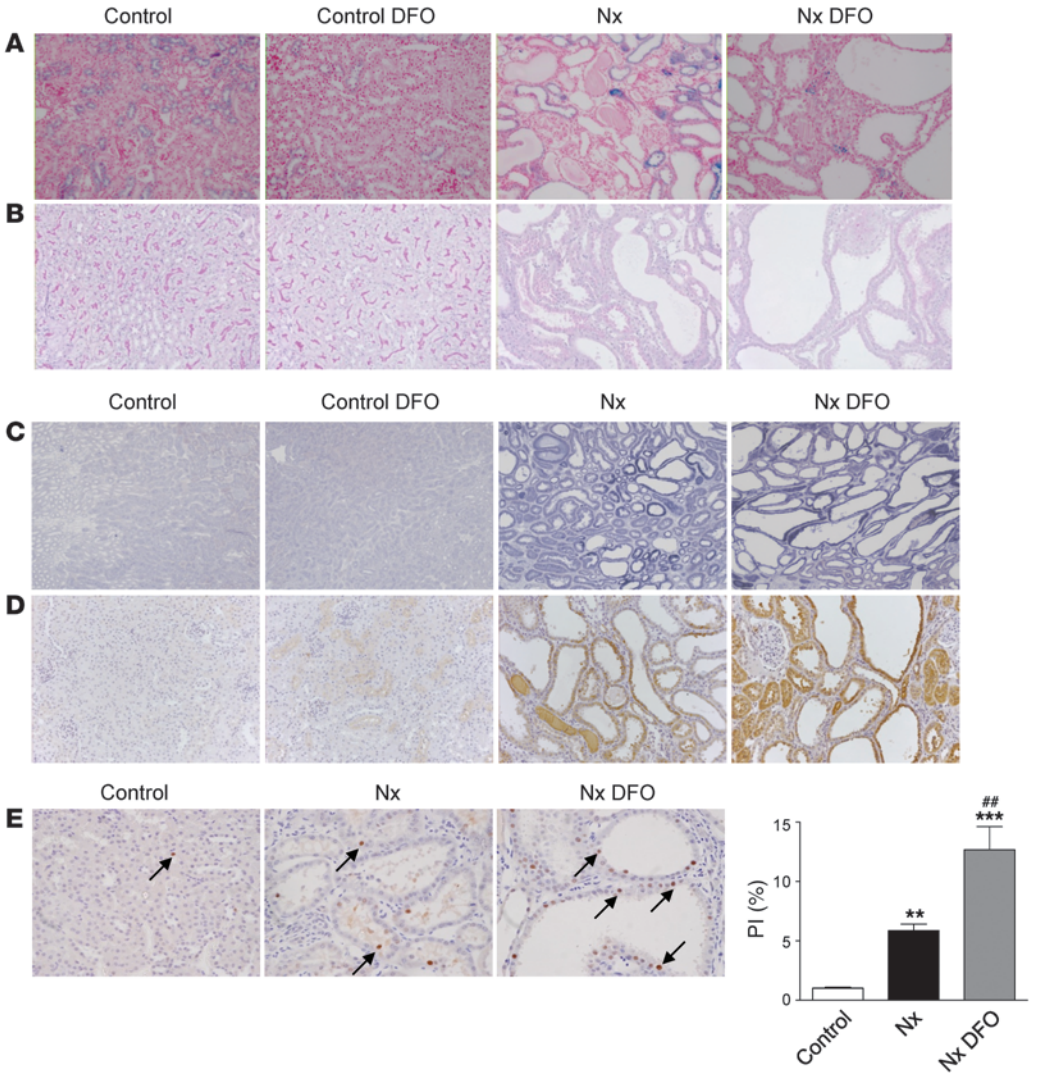

Figure 5
DFO increases Lcn2 expression and worsens renal lesions after nephron reduction. (**A**) Perls staining of kidneys from control and 75% Nx mice either treated or not with DFO. Original magnification, ×200. (**B**) Morphology of kidneys from control, DFO-treated control, Nx, and Nx DFO-treated mice, 2 months after surgery. Original magnification, ×200. (**C** and **D**) Lcn2 expression evaluated by (**C**) in situ hybridization (×100) and (**D**) immunohistochemistry (×200) in kidneys from control and Nx mice treated or not with DFO, 2 months after surgery. (**E**) DFO enhances cell proliferation after nephron reduction. PCNA staining (black arrows) and quantification of PI in kidneys from control and Nx mice, either treated or not with DFO. Original magnification, ×400. Because no differences were detected between wild-type and DFO-treated control mice, results for only 1 group are shown. Data are mean ± SEM; $n = 4–10$. ANOVA followed by Tukey-Kramer test: $^{**}P < 0.01$, $^{***}P < 0.001$, control versus Nx mice; $^{\#\#}P < 0.001$, Nx versus Nx DFO-treated mice.

ing cells (Supplemental 9). Thus, it appears that Lcn2 is an essential mediator of the mitogenic effect of EGF in renal tubular cells.

The dual effect of Lcn2 inactivation on apoptosis. Tubular growth reflects the balance between cell proliferation and cell loss by apoptosis. Both EGFR and Lcn2 have been implicated in the control of apoptosis (25, 29). TUNEL analysis revealed an increase in apoptosis in both tubules (Figure 9A) and glomeruli (Figure 9B) of wild-type mice as compared with control animals 2 months after nephron reduction. The number of TUNEL-positive cells was significantly reduced in *Lcn2*$^{-/-}$ mice in both glomerular and tubular structures (Figure 9, A and B). However, Lcn2 silencing did not significantly affect the number of apoptotic tubular mIMCD-3 cells, regardless of the presence of EGF (Figure 9B).

Discussion

Unbiased profiling analyses offer a powerful approach to uncover critical mediators and dissect novel molecular networks of complex biological processes such as CKD progression. By combining experimental models of CKD in mice from different genetic backgrounds with microarray analyses, we have established a pivotal role for Lcn2 in regulating the progression of CKD and cyst formation. Furthermore, we have defined an important pathophysiological mechanism by which Lcn2 mediates the mitogenic effect of EGFR, consistent with its role in cell proliferation in cystogenesis. Inhibition of this pathway by *Lcn2* gene inactivation or by the expression of a dominant negative EGFR isoform prevented lesion development in the transgenic mice. Conversely, overexpres-

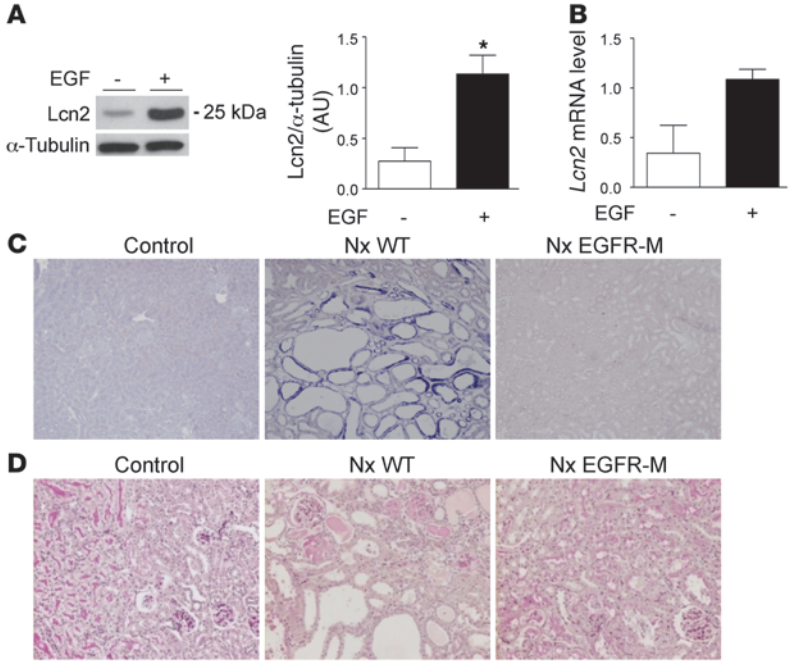

Figure 6

Lcn2 is a transcriptional target of EGFR. Lcn2 protein (**A**) and mRNA (**B**) expression in mIMCD-3 cells, 24 hours after EGF treatment. (**C** and **D**) Overexpression of a dominant negative EGFR isoform abolishes renal Lcn2 synthesis and prevents lesion development after nephron reduction. (**C**) *Lcn2* mRNA expression visualized by in situ hybridization (original magnification, ×100) and (**D**) renal morphology (PAS, ×200) of kidneys from control and 75% Nx wild-type and EGFR-M mice, 2 months after surgery. Data are mean ± SEM; n = 2–3 and 6–10 for in vitro and in vivo experiments, respectively. Wilcoxon test: *$P < 0.05$, vehicle- versus EGF-treated cells.

sion of Lcn2 significantly correlated with hyperproliferation and CKD progression in both mice and humans. We have further identified Hif-1α as a crucial intermediate between EGFR and Lcn2 upregulation. Collectively, these results elucidate what we believe to be a novel molecular pathway of CKD progression and show that Lcn2 acts as a growth-promoting factor whose overexpression identifies patients with rapid CKD progression.

Lcn2, like all members of the lipocalin superfamily, binds hydrophobic ligands; the ligand is thought to define the function of the protein. Lcn2 binds enterochelin (20), parabactin (20), and carboxymycobactin (30), which are siderophores produced by bacteria for the purpose of binding iron. The siderophore-chelating property of Lcn2 renders it a bacteriostatic agent (20). Consistent with this finding, *Lcn2* mutant mice have a profound defect in the defense against *E. coli* (19, 31) and *Mycobacterium tuberculosis* (32). Nonetheless, Lcn2 expression dramatically increases in several aseptic pathological conditions such as cancers (33), inflammatory diseases (34), and acute kidney injury (24), suggesting that Lcn2 may have other functions. To date, study of its noninfectious activities has focused on its effects on cell proliferation and/or apoptosis (24), but proof of these in a physiological setting in vivo has been lacking. Even in the case of acute kidney injury, a disease that is related to CKD, it remains unclear whether Lcn2 is a critical mediator of tubular changes (19). Hence, our work is the first clear demonstration to our knowledge that in vivo Lcn2 has a critical function in a pathological condition other than infection, namely serving as a growth regulator that mediates CKD progression. Our findings in mice and humans may be generally applicable to many forms of CKD, because Lcn2 is also expressed in obstructive uropathy (16), diabetic nephropathy (16), and in damaged kidneys of patients with IgA nephropathy (17) or HIV-associated nephropathy (18).

Our study shows that Lcn2, which is induced by EGFR, controls aberrant growth of renal tubules and cysts. Notably, we demonstrated that *Lcn2* gene inactivation inhibited proliferation of tubular cells, which led to a marked decrease in cyst formation in mice. Consistently, we identified cystic tubular epithelia as the major source of Lcn2 production. These data suggest that Lcn2 might act as a tubulogenic factor that controls cell growth. This is supported by additional evidence: first, Lcn2 induced tubular development in in vitro assays in the rat (35); second, Lcn2 infusion favored tubular regeneration after ischemic injury in mice (36); third, high LCN2 levels were associated with a higher rate of cystic growth in humans (37). This property was not limited to mammalian cells: Lpr-1, a newly identified lipocalin family member, controlled unicellular tube development in the excretory system of *Caenorhabditis elegans* (38). Our data also suggest that Lcn2 may modulate tubular shape by controlling both cell proliferation and apoptosis. In fact, the beneficial effect of *Lcn2* gene inactivation in mutant mice was accompanied by a decrease in tubular apoptosis, consistent with a previous observation in proximal tubule lacking *Pkd1*, a cystic disease–associated gene (39). However, this effect may be indirect, since Lcn2 silencing in vitro did not affect the number of apoptotic tubular cells. Whether the growth-promoting effect of Lcn2 is mediated by the binding of Lcn2 to a unique receptor, thus inducing a signaling cascade, or alternatively by iron mobilization, as suggested by the DFO experiments, remains to be elucidated.

In the present study we observed that *Lcn2* gene inactivation protected from glomerulosclerosis and interstitial fibrosis after nephron reduction, despite the fact that Lcn2 was expressed only by tubules. The mechanism for this observation remains unknown. It may result from the perfusion and filtration of serum Lcn2 that we found by immunostaining in the tubules. Alternatively, since injuries to tubular cells, i.e., proteinuria, result in the expression of tubular cytokines and growth factors that ultimately lead to mesangial cell proliferation and matrix synthesis (40), it is tempting to hypothesize a crosstalk between tubular and surrounding renal cells. Studies in transgenic mice strongly support this idea. For example, it has been observed that mice that overexpressed VEGF selectively in tubules developed interstitial fibrosis and glomerular disease (41). And we have previously shown that the overexpression of a dominant negative isoform of EGFR in proximal tubules prevented the development of glomerular and interstitial lesions after nephron reduction (26). On the other hand, it has been shown that interstitial scarring resulted in the loss of microvessels, which, in turn, impacted the adjacent unaffected glomeruli (42). It is worthy of note that the synthesis of paracrine mediators may increase in proliferating tubular cells (43). Hence, we speculate that by inhibiting tubular cell proliferation, Lcn2 might protect glomeruli and interstitium from lesions development.

Activation of EGFR has been implicated in the evolution of CKD. Overexpression of an active EGFR form, the c-erb-B2 receptor, induc-

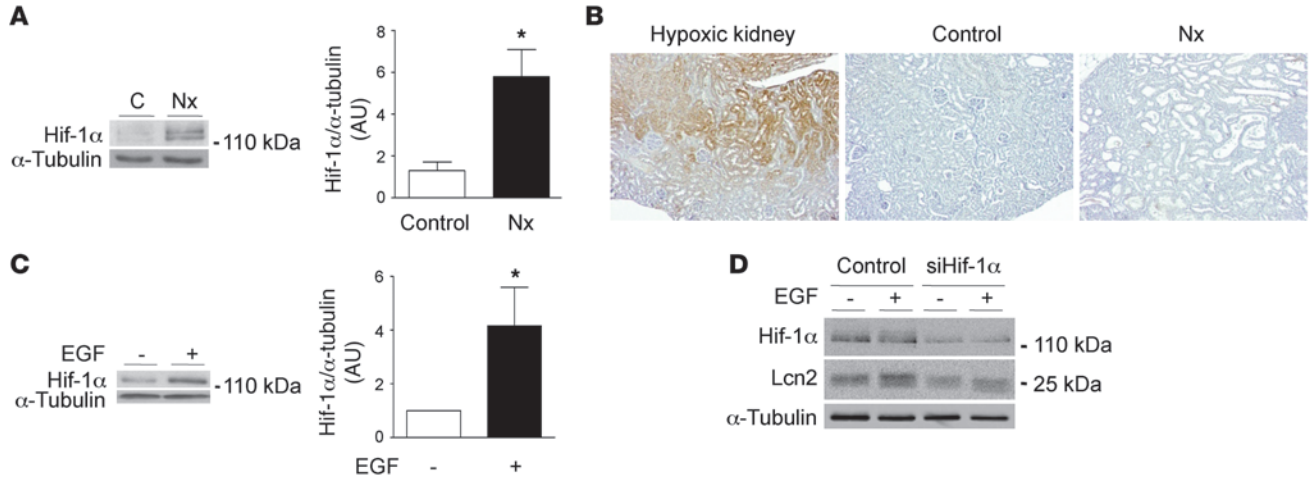

Figure 7

Hif-1α is a critical intermediate between EGFR and Lcn2. (**A**) Hif-1α protein expression and quantification in control and 75% Nx mice, 2 months after surgery. (**B**) Pimonidazole immunostaining in control and Nx mice, 2 months after surgery. Postischemic kidneys (2 hours clamping of renal pedicle) were used as positive hypoxic control. Original magnification, ×200. (**C**) Hif-1α protein expression and quantification in mIMCD-3 cells, 24 hours after EGF treatment. (**D**) Hif-1α silencing partially overcomes EGFR-induced Lcn2 upregulation. Hif-1α and Lcn2 protein expression in either mock- (Control) or Hif-1α siRNA–transfected (siHif-1α) mIMCD-3 cells, treated or not with EGF. Data are mean ± SEM; n = 2–6 and 6–10 for in vitro and in vivo experiments, respectively. Mann-Whitney U test: $^*P < 0.05$, control versus Nx mice; Wilcoxon test: $^*P < 0.05$, vehicle versus EGF-treated cells.

es tubular hyperplasia and the development of renal cysts in transgenic mice (44). Conversely, expression of a dominant negative EGFR isoform inhibits cell proliferation, leading to reduced tubular dilations after nephron reduction (26). Other genetic and pharmacological approaches have confirmed the key role of EGFR and cell proliferation in polycystic kidney diseases (45, 46), and overexpression and mislocalization of EGFR were observed in cystic epithelia of *jck* mice (15). On the other hand, we have previously established that EGFR acts as a central integrator of angiotensin II pathway, a potent mediator of CKD (47). While the exact molecular networks that mediate the deleterious effect of EGFR during CKD have not been yet elucidated, our data point to Lcn2 as the crucial transcriptional target of EGFR during cyst formation and glomerulosclerosis. It is worthy of note that a very recent study showed that Lcn2 is also required for c-erb-B2 receptor signaling in breast cancer (48). In addition, our data show that Hif-1α is a critical intermediate between EGFR and Lcn2, consistent with the finding that Lcn2 is upregulated in most pathological conditions characterized by hypoxia, such as ischemia or cancers (24, 33). Whether Hif-1α is more extensively involved in the control of *Lcn2* gene expression requires further investigations.

Clinical studies have suggested that urinary Lcn2 excretion might mark patients with the most severe clinical course (49), but whether Lcn2 is simply a marker of tubular damage or a key mediator of the deterioration process has been unknown. Our data now show a direct relationship between Lcn2 expression and disease progression and provide the first demonstration to our knowledge that Lcn2 is instrumental in CKD. CKD is a progressive disease, and there are many possible medical interventions over its course if the disease is recognized and treated in a timely manner. Current biomarkers of CKD progression, i.e., creatinine and albuminuria, have their limitations in terms of achieving this goal (50). An ideal biomarker should reflect tissue pathology, act as a critical component of disease, and be easily detectable by noninvasive approaches. By showing that Lcn2 unites these characteristics, we have provided strong evidence for the use of this molecule as a candidate biomarker of CKD progression.

In conclusion, we have uncovered what we believe to be a novel function of Lcn2 and highlighted its crucial role in the pathogenesis of progressive CKD. This is the first in vivo demonstration to our knowledge that Lcn2 acts as a growth regulator by mediating the mitogenic effect of EGFR signaling. Moreover, we have identified Lcn2 as one of the key effectors of renal damage and cystogenesis and one of the most promising biomarkers of CKD progression, worthy of study in large patient cohorts. We suspect that our findings will be critical in other pathological conditions that are also characterized by aberrant growth, such as cancers that demonstrate both EGFR activation and intensive Lcn2 expression (51, 52).

Methods

Animals. Mice used for these studies were FVB/N, C57BL/6, and B6D2F1 (Charles River); mutant *jck* bearing a *Nek8* mutation (The Jackson Laboratory); transgenic EGFR-M expressing a dominant negative isoform of EGFR under the control of kidney-specific type 1 γ-glutamyl transpeptidase promoter (26); and *Lcn2*$^{-/-}$ mice (19). *Lcn2*$^{-/-}$ mice on the FVB/N genetic background were obtained using a marker-assisted speed congenic strategy. Ninety-three microsatellite markers spanning each autosomal chromosome (average distance of 14.2 cM) were used to discriminate C57BL/6 and FVB/N alleles. Heterozygous C57BL/6 *Lcn2*$^{+/-}$ mice were bred with heterozygous *jck* mice to obtain double-homozygous transgenic *jck/Lcn2*$^{-/-}$ mice. All experiments were performed on 9-week-old females, except for *jck* mice that were studied 3 weeks after birth. Animals were fed ad libitum and housed at constant ambient temperature in a 12-hour light cycle. Animal procedures were approved by the Departmental Director of "Services Vétérinaires de la Préfecture de Police de Paris" and by the ethical committee of Université Paris Descartes.

Mice were subjected to 75% Nx or sham operation (controls), as previously described (26). After surgery, mice were fed a defined diet containing 30% casein and 0.5% sodium. Several groups of mice were investigated in complementary studies. For microarray studies, 6 and 9 mice from each strain were subjected to either sham operation or Nx, respectively. For Lcn2 time course analysis, 5–6 sham-operated and 4–8 Nx mice were studied at each

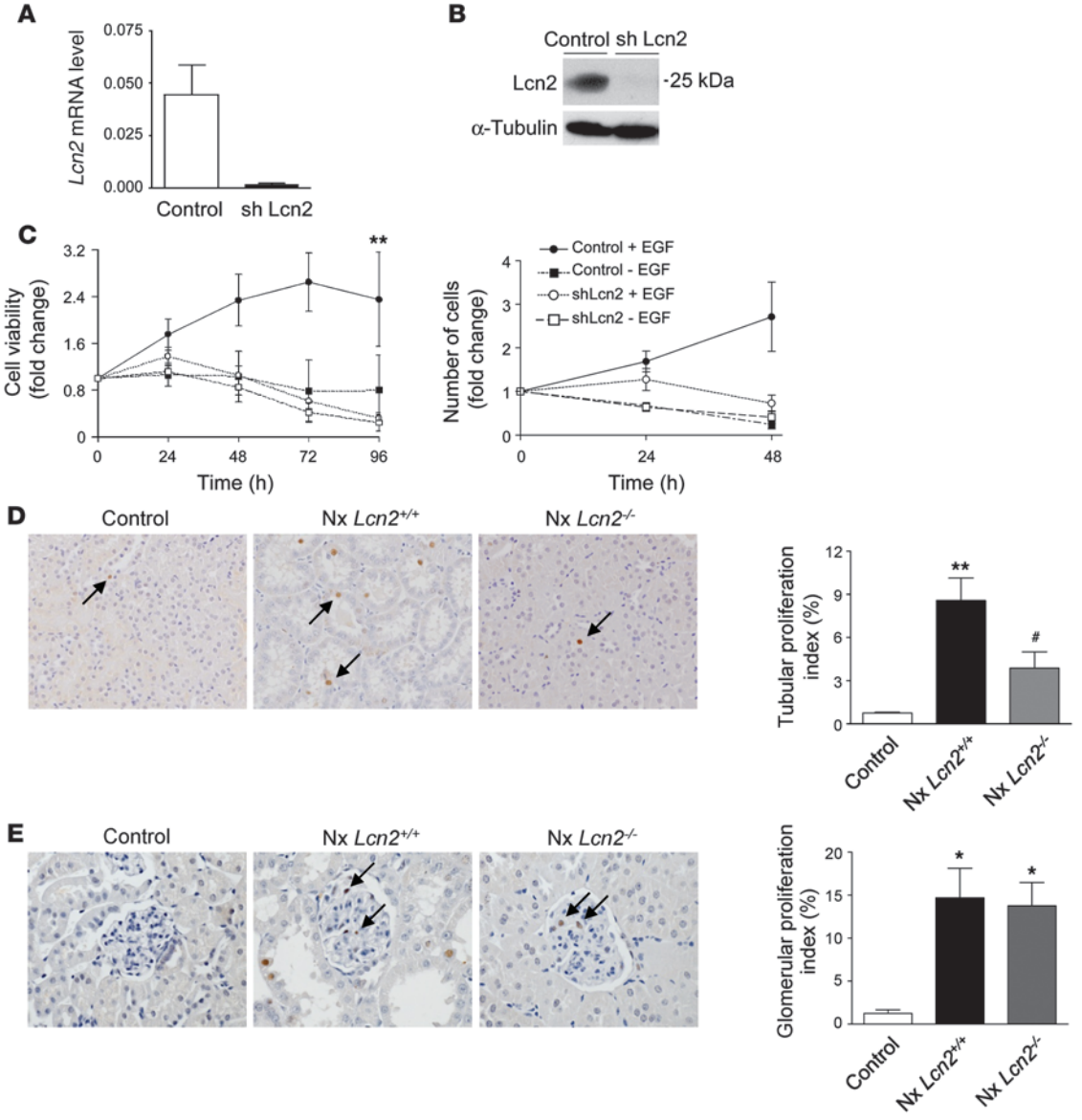

Figure 8

Lcn2 mediates the proliferative effect of EGFR. (**A** and **B**) Stable Lcn2 shRNA (shLcn2) inhibits Lcn2 expression in mIMCD-3 cell lines. mRNA (**A**) and protein (**B**) expression in shLcn2 cells as compared with scrambled shRNA cells (Control). (**C**) Cell proliferation assay (left panel) and cell counting (right panel) in scrambled shRNA and Lcn2 shRNA mIMCD-3 cells, treated or not with EGF. (**D**) PCNA staining (black arrows) and quantification of tubular proliferation in kidneys from control, 75% Nx *Lcn2*$^{+/+}$, and *Lcn2*$^{-/-}$ mice, 2 months after surgery. Original magnification, ×400. (**E**) PCNA staining (black arrow) and quantification of glomerular proliferation in kidneys from control, Nx *Lcn2*$^{+/+}$, and *Lcn2*$^{-/-}$ mice, 2 months after surgery. Original magnification, ×600. Because no differences were detected between wild-type and mutant control mice, results for only 1 group are shown. Data are mean ± SEM; n = 3–4 and 6–10 for in vitro and in vivo experiments, respectively. ANOVA followed by Tukey-Kramer test: $^{**}P < 0.01$, control versus shLcn2 cell lines; $^{*}P < 0.05$, $^{**}P < 0.01$, control versus Nx mice; $^{\#}P < 0.05$, Nx *Lcn2*$^{+/+}$ versus Nx *Lcn2*$^{-/-}$ mice.

time point. Transgenic studies employed EGFR-M or *Lcn2*$^{-/-}$ mice and wild-type littermates; for each group, 4–6 mice were subjected to sham operation and 10–16 mice to nephron reduction. For iron chelation experiments, 5 sham-operated and 6 Nx mice were injected with 100 mg/kg/d DFO (Sigma-Aldrich) by subcutaneous osmotic minipumps (2004, Alzet) for 2 months. For hypoxyprobe experiments, 6 sham-operated and 6 Nx mice were injected intraperitoneally with 60 mg/kg pimonidazole (Chemicon) 2 hours before sacrifice. Postischemic kidneys (2 hours renal pedicle clamping) were used as positive hypoxic controls.

Mice were sacrificed 2 months after surgery. In addition, for Lcn2 time course study, mice were also sacrificed at 4 and 6 weeks after surgery. One week before sacrifice, blood pressure was recorded in both sham-operated (n = 3) and subtotally nephrectomized (n = 6) awake *Lcn2*$^{+/+}$ and *Lcn2*$^{-/-}$ mice for 2 consecutive days, using tail-cuff plethysmography and PowerLab/4SP software (AD Instruments). Urine samples were also collected using metabolic cages from 6 mice of each experimental group over the course of 24 hours. At the time of sacrifice, the kidney was removed for morphological, protein, and mRNA studies.

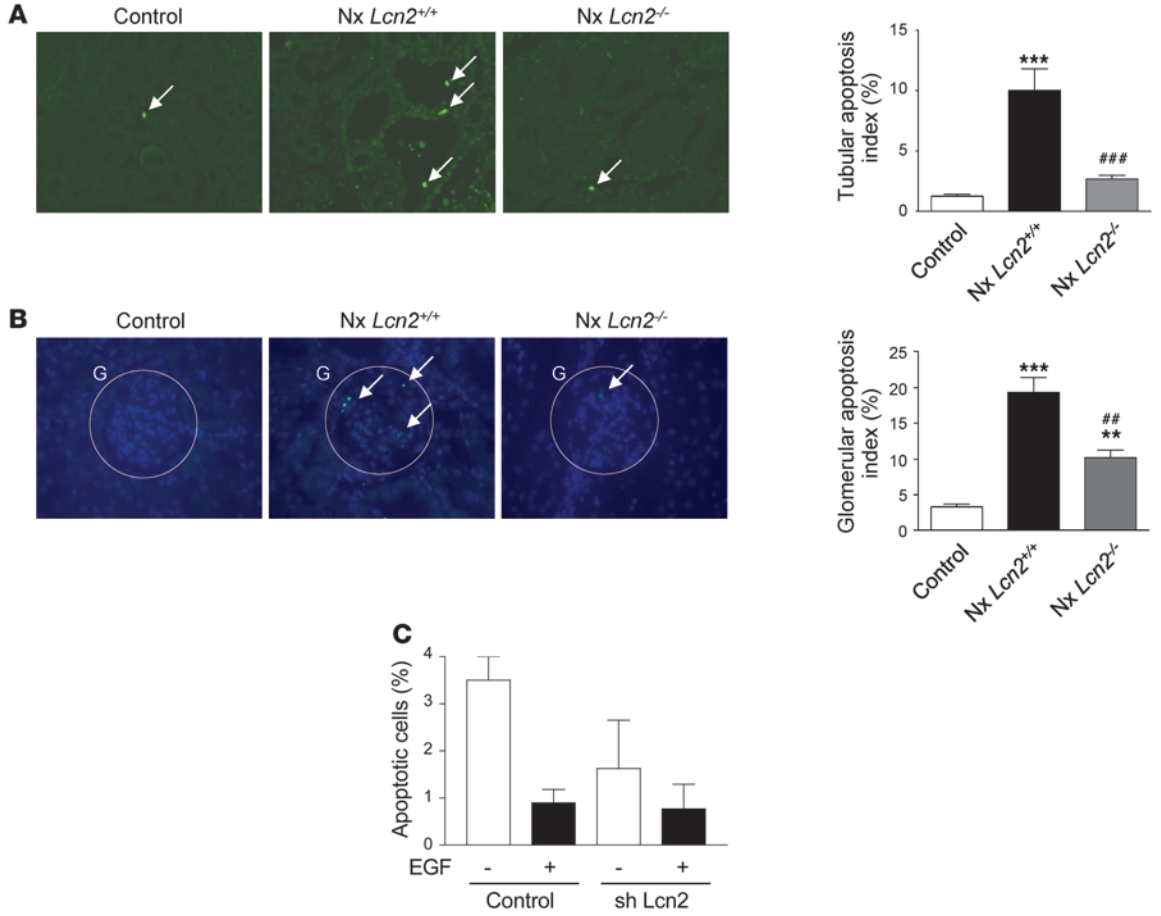

Figure 9
Impact of *Lcn2* inactivation on apoptosis. (**A**) TUNEL assay and quantification of TUNEL-positive tubular cells (white arrows) in kidneys from control, 75% Nx *Lcn2*$^{+/+}$, and *Lcn2*$^{-/-}$ mice, 2 months after surgery. Original magnification, ×400. (**B**) TUNEL assay and quantification of TUNEL-positive glomerular cells (white arrows) in kidneys from control, Nx *Lcn2*$^{+/+}$, and *Lcn2*$^{-/-}$ mice, 2 months after surgery. G, glomerulus. Original magnification, ×600. Because no differences were detected between wild-type and mutant control mice, results for only 1 group are shown. (**C**) Cell apoptosis quantification in scrambled shRNA and Lcn2 shRNA mIMCD-3 cells, 24 hours after EGF treatment. Data are mean ± SEM; $n = 3$ and 4 for in vitro and in vivo experiments, respectively. ANOVA followed by Tukey-Kramer test: $^{**}P < 0.01$, $^{***}P < 0.001$, control versus Nx mice; $^{\#\#}P < 0.01$, $^{\#\#\#}P < 0.001$, Nx *Lcn2*$^{+/+}$ versus Nx *Lcn2*$^{-/-}$ mice.

Clinical samples. The study was conducted on 87 subjects with ADPKD (40 male, 47 female; mean age 52.4 years, range 24.7–79.2 years). The mean serum creatinine level of patients was 252 ± 169.9 mmol/l, and the eGFR value (assessed using the MDRD formula; ref. 53) was 33 ± 20 ml/min/1.73 m^2. Of the 87 patients, 76 were hypertensive under treatment. The decline in renal function was evaluated retrospectively over 6 years, then patients were divided into 2 groups: slow progressors (eGFR decline <4.5 ml/min/1.73 m^2 per year; mean, 2.4 ± 0.1; $n = 52$) or fast progressors (eGFR decline >4.5 ml/min/1.73 m^2 per year; mean, 6.0 ± 0.2; $n = 35$).

Kidneys from patients with ADPKD ($n = 9$), oligomeganephronia ($n = 11$), and IgA nephropathy ($n = 12$) were analyzed for LCN2 expression. Normal kidneys not used for transplantation or tumor-free pole of kidneys removed for carcinoma were used as controls ($n = 9$).

This protocol was approved by the Hospital Plan for Clinical Research (PHRC) program of the French Ministry of Health. Informed consent was obtained from volunteers before enrollment in the study.

Cells. For siRNA transfection experiments, transient inactivation of Hif-1α expression in mIMCD-3 cells was achieved using siRNA SMARTpool from Dharmacon according to the manufacturer's recommendations. Cells were transfected with siRNA (100 nM) using DharmaFECT4 siRNA Transfection Reagent (Thermo Fisher Scientific). Eight hours after transfection, cells were serum starved for 12 hours and then treated with 40 ng/ml EGF (R&D Systems) in serum-deprived medium for 48 hours.

For shRNA transfections, mIMCD-3 cells were stably transfected with pSuppressor Retro vector (Imgenex) containing an shRNA for Lcn2 or a scramble oligonucleotide (Dharmacon). The Lcn2 shRNA sequence contains either the cloning nucleotides 5′-GGAAATATGCACAGGTATC-3′ or 5′-GCTACTGGATCAGAACATT-3′ followed by a 9-base loop and the inverted cloning sequence. In the scramble sequence, the cloning sequence is replaced by 5′-GAGCGTACCAGATTAAAGT-3′ or 5′-GATTCGACCAGACATGTAT-3′. Cells stably transfected were maintained in DMEM/HamF12 medium containing 10% FBS.

For EGF experiments, cells were serum starved for 18 hours and then treated with 40 ng/ml EGF in serum-deprived medium for 24–96 hours. Cells were collected at 24 hours for Lcn2 assay and apoptosis experiments and at 24–96 hours for proliferation experiments.

cDNA microarray. RNAs were obtained from whole kidneys of 9 Nx mice from each strain using RNeasy Midi Kit (QIAGEN) according to the

manufacturer's protocol. RNAs were reverse transcribed and labeled with either cyanine Cy-3 or Cy-5. FVB/N Cy3-cDNAs and B6D2F1 Cy5-cDNAs (and, conversely, FVB/N Cy5- and B6D2F1 Cy3-cDNAs) were cohybridized on mouse cDNA microarrays containing 5,579 cDNAs including expressed sequence tags (Genopole). Preparations of RNAs and cDNAs and hybridization were performed according to the Genopole protocol, as previously reported (54). Six arrays were hybridized. For each array, the RNAs from 3 mice were pooled. Hybridized microarrays were scanned and images were analyzed using GenepixPro 4.0 software (Molecular Devices) by the Genopole microarray facility.

Real-time RT-PCR. Lcn2 mRNA was detected in mouse kidneys and mIMCD-3 cells by real-time RT-PCR using an ABI PRISM 7700 Sequence Detection system (Applied Biosystems). Primers (Eurogentec) were as follows: Lcn2 forward 5′-GGACCAGGGCTGTCGCTACT-3′ and reverse 5′-GGTGGCCACTTGCACATTGT-3′; Hif-1α (i) forward 5′-CCTGGAAACGAGTGAAAGGATTC-3′ and reverse 5′-GCATGCTAAATCGGAGGGTATTAA-3′; Hif-1α (ii) forward 5′-TCACCAGACAGAGCAGGAAAGAG-3′ and reverse 5′-GGCAGACAGGTTAAGGCTCCTT-3′. Gapdh and Sdha were used as the normalization controls in kidneys and cells, respectively.

Renal function and morphology. For mouse samples, proteinuria and blood urea nitrogen were measured using an Olympus multiparametric analyzer (Instrumentation Laboratory), while serum creatinine was evaluated by HPLC. For human samples, creatininuria and albuminuria were measured using a Hitachi 917 analyzer (Roche Diagnostics).

Kidneys were fixed in 4% paraformaldehyde and paraffin embedded, and 4-μm sections were stained with PAS, Masson's trichrome, H&E, and picrosirius red. Ferric iron deposits were detected using Prussian blue staining according to Perls reaction. The degree of glomerular and interstitial lesions was evaluated using semiquantitative score methodology as previously described (7). The degree of tubular lesions was quantified using a Nikon digital camera Dx/m/1200 and Lucia software (Laboratory Imaging Ltd.). Ten randomly selected microscopic fields (×200) were scored. For *jck* mice, the entire section was quantified at ×100 magnification. The tubular score was expressed as the ratio between the tubular dilation surface and the total section area.

In situ hybridization. In situ hybridization was carried out on 8-μm sections of paraffin-embedded mouse kidneys using digoxigenin-labeled riboprobe corresponding to nucleotides 80–641 of the mouse Lcn2 sequence (NM_008491). Riboprobe was synthesized using reagents from Roche, according to the manufacturer's instructions.

Western blot analysis. Western blots were performed as previously described (12) using either a goat antibody to mouse Lcn2 (R&D Systems) at 1:1,000 in 1% milk/TBST or a rabbit antibody to mouse Hif-1α or Hif-2α (Novus Biologicals) at 1:500 or 1:200, respectively, in 5% milk/TBST followed by either a rabbit horseradish peroxidase–conjugated anti-goat antibody at 1:10,000 (Dako) or a donkey horseradish peroxidase–conjugated anti-rabbit antibody at 1:2,000 (Amersham). Mouse monoclonal α-tubulin antibody (Sigma-Aldrich) was used as control. Protein extracts from kidneys of *Lcn2*$^{-/-}$ mice were used to confirm antibody specificity.

Immunohistochemistry. For mouse samples, 4-μm sections of paraffin-embedded kidneys were incubated with a goat anti-mouse Lcn2 antibody (R&D Systems) at 1:300, followed by a rabbit anti-goat biotinylated antibody (Dako) at 1:200. Biotinylated antibodies were detected using HRP-labeled streptavidin (Dako) at 1:500 and 3-3′-diamino-benzidine-tetrahydrochloride (DAB) revelation.

For colocalization experiments, lotus tetragonolobus lectin (LTL) was detected using biotinylated LTL (Vector) at 1:50, followed by HRP-labeled streptavidin at 1:500. For Tamm-Horsfall staining, mouse kidney sections were incubated with a goat anti–Tamm-Horsfall antibody (Biogenesis) diluted 1:200, followed by a biotinylated goat antibody (Dako) at 1:500 and HRP-labeled streptavidin at 1:500. For aquaporin 2 staining, sections were incubated with a rabbit anti–aquaporin 2 antibody (Sigma-Aldrich) at 1:400, followed by donkey HRP-conjugated anti-rabbit antibody (Amersham) at 1:300. DAB staining was used to detect antibodies.

For hypoxyprobe staining, 4-μm sections of paraffin-embedded kidneys were treated with pronase 0.01%, then incubated with an anti-hypoxyprobe adducts antibody (Chemicon) 1:200, followed by a biotinylated mouse antibody (Dako) at 1:500 and HRP-labeled streptavidin at 1:500 and subjected to DAB revelation.

For human samples, 4-μm sections of paraffin-embedded kidneys were incubated with a goat anti-human LCN2 antibody (R&D Systems) at 1:100, followed by an HRP-labeled rabbit anti-goat antibody (Dako) at 1:100 and DAB revelation.

Cell proliferation assay. Proliferative cells were detected in mouse kidney using PCNA or Ki-67 immunostaining. For PCNA staining, 4-μm sections of paraffin-embedded kidneys were incubated with a mouse anti-PCNA antibody (Dako) at 1:50, followed by a sheep HRP-conjugated anti-mouse antibody (Amersham) at 1:100. For Ki-67 staining, 4-μm kidney sections were incubated with a mouse anti–human Ki-67 (BD Biosciences — Pharmingen), followed by a biotinylated mouse antibody (Vector) at 1:400 and a HRP-labeled streptavidin at 1:1,000. Staining was revealed by DAB. The tubular proliferation index (PI) was calculated as the number of PCNA-positive (or Ki-67–positive) nuclei for the total number of tubular nuclei in 10 randomly selected fields. The glomerular PI was calculated as the number of glomeruli with at least 1 PCNA-positive nucleus for the total number of glomeruli. In vitro, proliferation was evaluated by counting the cell number or by using CellTiter 96 AQ_{ueous} Cell Proliferation Reagent (Promega) according to the manufacturer's instructions.

Apoptosis assay. Apoptosis was detected in 4-μm sections of paraffin-embedded kidneys by TUNEL assay using the In Situ Cell Death Detection Kit (Roche) according to the manufacturer's protocol. The number of apoptotic cells was determined as the number of TUNEL-positive nuclei per tubule in 20 randomly selected fields. The glomerular apoptotic index was calculated as the number of glomeruli with at least 1 TUNEL-positive nucleus for the total number of glomeruli. In vitro, apoptotic cells were detected by DAPI staining, and the apoptotic index was calculated as the number of apoptotic-positive nuclei for the total number of nuclei in 10 randomly selected fields.

Measurement of urinary LCN2. Fresh urine was collected with protease inhibitors, centrifuged at 805 *g* at 4°C for 5 minutes, and the supernatant was removed and stored at –80°C. LCN2 was measured using ELISA (AntibodyShop). Specimens, standards, and reagents were prepared according to the manufacturer's instructions. LCN2 levels were expressed as nanograms per milligram of creatinine. All experiments were performed in duplicate.

Statistics. Data are expressed as mean ± SEM. Differences between the experimental groups were evaluated using ANOVA, followed when significant ($P < 0.05$) by the Tukey-Kramer test. When only 2 groups were compared, Mann-Whitney *U* or Wilcoxon tests were used. The Pearson's correlation coefficient was used to test correlation between variables. For microarray experiments, results are expressed as a $\log_2$ of the ratio of Cy5 to Cy3. Genes with a false discovery rate (FDR) less than 0.05 (using the Benjamini-Hochberg procedure) and a fold change greater than 1.5 were considered significant. The statistical analysis was performed using GraphPad Prism software.

Acknowledgments

We are grateful to Sophie Berissi and Nicolas Cagnard for technical assistance. We are grateful to Genopole d'Evry, Laurent Beck, and Thierry Gilbert for microarrays, pSuppressor Retro vector, and in situ hybridization protocol, respectively. We thank Françoise Leviel for serum creatinine measurement by HPLC and David De Brauwere and the Biochemistry department of Necker Hospital for bio-

logical assays on patients' urine. We thank Marco Pontoglio and Corinne Antignac for critical advice and Annette Bonnell for text revision. This work was supported by INSERM, Université Paris Descartes, AP-HP, Subvention AMGEM/Societé de Néphrologie, AURA (Paris), Agence Nationale Recherche (ANR-06-PHYSIO-029-01 grant), Fondation de la Recherche Médicale (DEQ20061107968 grant), AIRG, and Fondation Groupama. J. Barasch is supported by grants from the NIH and the March of Dimes.

Received for publication May 18, 2010, and accepted in revised form August 9, 2010.

Address correspondence to: Fabiola Terzi, INSERM U845, Team: Mechanisms and Therapeutic Strategies in Chronic Nephropathies, Hôpital Necker Enfants Malades, Tour Lavoisier, 6ème étage, 149 Rue de Sèvres, 75015 Paris, France. Phone: 33.1.44495245; Fax: 33.1.44490290; E-mail: fabiola.terzi@inserm.fr.

1. Collins AJ, et al. US Renal Data System: excerpts from the USRDS 2005 Annual Data Report. *Am J Kidney Dis.* 2006;47(suppl 1):S1–S286.
2. Meguid El Nahas A, Bello AK. Chronic kidney disease: the global challenge. *Lancet*. 2005;365(9456):331–340.
3. Kidney and Urologic Diseases Statistics for the United States. National Kidney and Urologic Diseases Information Clearinghouse (NKUDIC) Web Site. http://kidney.niddk.nih.gov/kudiseases/pubs/kustats/index.htm. Accessed August 10, 2010.
4. Hostetter TH. Progression of renal disease and renal hypertrophy. *Annu Rev Physiol*. 1995;57:263–278.
5. Terzi F, et al. Subtotal but not unilateral nephrectomy induces hyperplasia and protooncogene expression. *Am J Physiol*. 1995;268(5 pt 2):F793–F801.
6. Kliem V, et al. Mechanisms involved in the pathogenesis of tubulointerstitial fibrosis in 5/6-nephrectomized rats. *Kidney Int*. 1996;49(3):666–678.
7. Pillebout E, et al. JunD protects against chronic kidney disease by regulating paracrine mitogens. *J Clin Invest*. 2003;112(6):843–852.
8. Remuzzi G, Benigni A, Remuzzi A. Mechanisms of progression and regression of renal lesions of chronic nephropathies and diabetes. *J Clin Invest*. 2006;116(2):288–296.
9. Esposito C, He CJ, Striker GE, Zalups RK, Striker LJ. Nature and severity of the glomerular response to nephron reduction is strain-dependent in mice. *Am J Pathol*. 1999;154(3):891–897.
10. Kren S, Hostetter TH. The course of the remnant kidney model in mice. *Kidney Int*. 1999;56(1):333–337.
11. Ma LJ, Fogo AB. Model of robust induction of glomerulosclerosis in mice: importance of genetic background. *Kidney Int*. 2003;64(1):350–355.
12. Pillebout E, et al. Proliferation and remodeling of the peritubular microcirculation after nephron reduction: association with the progression of renal lesions. *Am J Pathol*. 2001;159(2):547–560.
13. Flower DR, North AC, Attwood TK. Mouse oncogene protein 24p3 is a member of the lipocalin protein family. *Biochem Biophys Res Commun*. 1991;180(1):69–74.
14. Schlehuber S, Skerra A. Lipocalins in drug discovery: from natural ligand-binding proteins to "anticalins". *Drug Discov Today*. 2005;10(1):23–33.
15. Smith LA, et al. Development of polycystic kidney disease in juvenile cystic kidney mice: insights into pathogenesis, ciliary abnormalities, and common features with human disease. *J Am Soc Nephrol*. 2006;17(10):2821–2831.
16. Kuwabara T, et al. Urinary neutrophil gelatinase-associated lipocalin levels reflect damage to glomeruli, proximal tubules, and distal nephrons. *Kidney Int*. 2009;75(3):285–294.
17. Ding H, et al. Urinary neutrophil gelatinase-associated lipocalin (NGAL) is an early biomarker for renal tubulointerstitial injury in IgA nephropathy. *Clin Immunol*. 2007;123(2):227–234.
18. Paragas N, et al. Urinary NGAL marks cystic disease in HIV-associated nephropathy. *J Am Soc Nephrol*. 2009;20(8):1687–1692.
19. Berger T, et al. Lipocalin 2-deficient mice exhibit increased sensitivity to Escherichia coli infection but not to ischemia-reperfusion injury. *Proc Natl Acad Sci U S A*. 2006;103(6):1834–1839.
20. Goetz DH, Holmes MA, Borregaard N, Bluhm ME, Raymond KN, Strong RK. The neutrophil lipocalin NGAL is a bacteriostatic agent that interferes with siderophore-mediated iron acquisition. *Mol Cell*. 2002;10(5):1033–1043.
21. Nankivell BJ, Boadle RA, Harris DC. Iron accumulation in human chronic renal disease. *Am J Kidney Dis*. 1992;20(6):580–584.
22. Harris DC, Tay YC, Chen J, Chen L, Nankivell BJ. Mechanisms of iron-induced proximal tubule injury in rat remnant kidney. *Am J Physiol*. 1995;269(2 pt 2):F218–F224.
23. Igarashi P, Somlo S. Genetics and pathogenesis of polycystic kidney disease. *J Am Soc Nephrol*. 2002;13(9):2384–2398.
24. Schmidt-Ott KM, et al. Dual action of neutrophil gelatinase-associated lipocalin. *J Am Soc Nephrol*. 2007;18(2):407–413.
25. Zeng F, Singh AB, Harris RC. The role of the EGF family of ligands and receptors in renal development, physiology and pathophysiology. *Exp Cell Res*. 2009;315(4):602–610.
26. Terzi F, et al. Targeted expression of a dominant-negative EGF-R in the kidney reduces tubulointerstitial lesions after renal injury. *J Clin Invest*. 2000;106(2):225–234.
27. Semenza GL. Targeting HIF-1 for cancer therapy. *Nat Rev Cancer*. 2003;3(10):721–732.
28. Gunaratnam L, Bonventre JV. HIF in kidney disease and development. *J Am Soc Nephrol*. 2009;20(9):1877–1887.
29. Devireddy LR, Gazin C, Zhu X, Green MR. A cell-surface receptor for lipocalin 24p3 selectively mediates apoptosis and iron uptake. *Cell*. 2005;123(7):1293–1305.
30. Holmes MA, Paulsene W, Jide X, Ratledge C, Strong RK. Siderocalin (Lcn 2) also binds carboxymycobactins, potentially defending against mycobacterial infections through iron sequestration. *Structure*. 2005;13(1):29–41.
31. Flo TH, et al. Lipocalin 2 mediates an innate immune response to bacterial infection by sequestrating iron. *Nature*. 2004;432(7019):917–921.
32. Saiga H, et al. Lipocalin 2-dependent inhibition of mycobacterial growth in alveolar epithelium. *J Immunol*. 2008;181(12):8521–8527.
33. Yang J, Moses MA. Lipocalin 2: a multifaceted modulator of human cancer. *Cell Cycle*. 2009;8(15):2347–2352.
34. Borregaard N, Cowland JB. Neutrophil gelatinase-associated lipocalin, a siderophore-binding eukaryotic protein. *Biometals*. 2006;19(2):211–215.
35. Yang J, et al. An iron delivery pathway mediated by a lipocalin. *Mol Cell*. 2002;10(5):1045–1056.
36. Mori K, et al. Endocytic delivery of lipocalin-siderophore-iron complex rescues the kidney from ischemia-reperfusion injury. *J Clin Invest*. 2005;115(3):610–621.
37. Bolignano D, et al. Neutrophil gelatinase-associated lipocalin in patients with autosomal-dominant polycystic kidney disease. *Am J Nephrol*. 2007;27(4):373–378.
38. Stone CE, Hall DH, Sundaram MV. Lipocalin signaling controls unicellular tube development in the Caenorhabditis elegans excretory system. *Dev Biol*. 2009;329(2):201–211.
39. Wei F, et al. Neutrophil gelatinase-associated lipocalin suppresses cyst growth by Pkd1 null cells in vitro and in vivo. *Kidney Int*. 2008;74(10):1310–1318.
40. Tang S, Leung JC, Tsang AW, Lan HY, Chan TM, Lai KN. Transferrin up-regulates chemokine synthesis by human proximal tubular epithelial cells: implication on mechanism of tubuloglomerular communication in glomerulopathic proteinuria. *Kidney Int*. 2002;61(5):1655–1665.
41. Hakroush S, et al. Effects of increased renal tubular vascular endothelial growth factor (VEGF) on fibrosis, cyst formation, and glomerular disease. *Am J Pathol*. 2009;175(5):1883–1895.
42. Fine LG, Norman JT. Chronic hypoxia as a mechanism of progression of chronic kidney diseases: from hypothesis to novel therapeutics. *Kidney Int*. 2008;74(7):867–872.
43. Strutz F, et al. Basic fibroblast growth factor expression is increased in human renal fibrogenesis and may mediate autocrine fibroblast proliferation. *Kidney Int*. 2000;57(4):1521–1538.
44. Stocklin E, Botteri F, Groner B. An activated allele of the c-erbB-2 oncogene impairs kidney and lung function and causes early death of transgenic mice. *J Cell Biol*. 1993;122(1):199–208.
45. Richards WG, Sweeney WE, Yoder BK, Wilkinson JE, Woychik RP, Avner ED. Epidermal growth factor receptor activity mediates renal cyst formation in polycystic kidney disease. *J Clin Invest*. 1998;101(5):935–939.
46. Sweeney WE, Chen Y, Nakanishi K, Frost P, Avner ED. Treatment of polycystic kidney disease with a novel tyrosine kinase inhibitor. *Kidney Int*. 2000;57(1):33–40.
47. Lautrette A, et al. Angiotensin II and EGF receptor cross-talk in chronic kidney diseases: a new therapeutic approach. *Nat Med*. 2005;11(8):867–874.
48. Leng X, et al. Inhibition of lipocalin 2 impairs breast tumorigenesis and metastasis. *Cancer Res*. 2009;69(22):8579–8584.
49. Nickolas TL, Barasch J, Devarajan P. Biomarkers in acute and chronic kidney disease. *Curr Opin Nephrol Hypertens*. 2008;17(2):127–132.
50. Lemley KV. An introduction to biomarkers: applications to chronic kidney disease. *Pediatr Nephrol*. 2007;22(11):1849–1859.
51. Shepard HM, Brdlik CM, Schreiber H. Signal integration: a framework for understanding the efficacy of therapeutics targeting the human EGFR family. *J Clin Invest*. 2008;118(11):3574–3581.
52. Devarajan P. Neutrophil gelatinase-associated lipocalin: new paths for an old shuttle. *Cancer Ther*. 2007;5(B):463–470.
53. Levey AS, Bosch JP, Lewis JB, Greene T, Rogers N, Roth D. A more accurate method to estimate glomerular filtration rate from serum creatinine: a new prediction equation. Modification of Diet in Renal Disease Study Group. *Ann Intern Med*. 1999;130(6):461–470.
54. Diarra-Mehrpour M, et al. Prion protein prevents human breast carcinoma cell line from tumor necrosis factor alpha-induced death. *Cancer Res*. 2004;64(2):719–727.